Supporting Information

Harris et al. 10.1073/pnas.1200352109

SI Materials and Methods

Plant Material and Growth Conditions. All WT and mutant *Arabidopsis* used were of the Columbia (Col-0) ecotype, and seedlings were germinated and grown as previously described (1). Inhibitors were dissolved in dimethylsufoxide (DMSO) and added to media so that DMSO never exceeded 0.1% (vol/vol). Isoxaben was purchased from Chem Service Inc. Chemical libraries used and screening conditions have been described in ref. 1 and supplemental on-line material. *ixr1-2* was obtained from the Arabidopsis Biological Resource Center at Ohio State University. Transgenic plants expressing various florescent protein tagged genes or gene knockouts were developed by reciprocal crossing and have been described elsewhere (1–3).

Map-Based Cloning of the Quinoxyphen Resistance Locus. Bulked segregant analysis and fine-mapping narrowed the location of the quinoxyphen resistant locus to an 830-kb region between markers UKY3 and NGA1139 that contained the *AtCESA1* gene. Details about the markers are available at The Arabidopsis Information Resource (www.arabidopsis.org). Growth of seed from the F_2 mapping population indicated that heterozygote individuals possessed some degree of resistance to 5.0 μM quinoxyphen as shown by the growth of radially swollen roots suggesting that the *aegeus* mutation confers a semidominant phenotype. To confirm that the mutation found in the *aegeus* mutant was responsible for the quinoxyphen-resistance phenotype, the WT *AtCESA1* gene was transformed into the aegeus mutant. T_2 progeny of the *aegeus* mutants transformed with the *AtCESA1* gene segregated for susceptibility on media containing 100 μM quinoxyphen, where only plants homozygous for the *aegeus* mutation can grow.

Cellulose Content Analysis and [^{14}C]-Glucose Incorporation Assays. Total cellulose content was determined for 7-d-old dark-grown hypocotyls and 8-wk-old stems (5 mg) according to Updegraff (4). For [^{14}C]-glucose incorporation assays, seeds were germinated and grown in multiwell tissue culture plates at 21 °C in the dark in 2 mL of sterile, liquid MS media containing 0.5% [wt/vol] glucose. After 3 d, the media was replaced with fresh MS media without glucose and containing either 0.05% DMSO or 50 μM quinoxyphen. After 1 h of preincubation with or without inhibitor, 0.5 μCi/mL [^{14}C]-glucose (American Radiolabeled Chemicals Inc.) was added to each well. The seedlings were incubated for 2 h in the dark at 21 °C and then washed and extracted as described (5).

Microscopy. Seedlings expressing GFP::CESA3 or YFP::CESA6 were grown in the dark for 3 d and imaged using spinning disk confocal microscopy, as described previously (6) except a DMI6000 B inverted microscope with Adaptive Focus Control (Leica) was used. Cells in the upper hypocotyl were imaged at 5-s intervals for 6 min at the plasma membrane. Images were processed to minimize signal from underlying Golgi bodies and to enhance particles at the plasma membrane. A 5-frame running average was applied to the series followed by rolling ball background subtraction (2 pixel radius). Then an FFT bandpass filter was applied to enhance structures of 2–3 pixels (0.32–0.49 μm). Data were analyzed with Imaris software (Bitplane). Cellulose synthase (CESA) particles were detected using the Spots module (estimated diameter = 0.5 μm) and tracked using the Autoregressive Motion algorithm (maximum frame-to-frame distance = 0.067 μm, maximum gap size = 1 frame). CESA velocity was calculated as total displacement divided by duration for tracks with a duration ≥18 frames (90 s) and straightness ≥0.75. Univariate analysis of variance, with Bonferroni post hoc tests, was performed using SPSS 19 software (IBM) to compare CESA velocities from different genotypes.

Chemical Screening Conditions. Chemical libraries used and screening conditions have been described (1). In brief, approximately 10 sterilized *Arabidopsis* seeds were sown per well, and the plates were incubated in 24-h light (50 μE/m^2 per s) at 21 °C for 3 d for initial isolation of quinoxyphen. Growth was compared to control wells that contained the same amount of DMSO. Plates were visually scored after 3 d of growth by inspecting each well with a dissecting microscope. Structural analogs were determined using the ChemMine website (http://bioweb.ucr.edu/ChemMine) (7) and purchased from ChemBridge. Screening of these compounds for increased potency or any change in phenotype involved germinating seedlings on plates containing half-strength Murashige and Skoog (MS) mineral salts (Sigma-Aldrich), 0.8% agar and after which grown under continuous light (200 μE/m^2 per s) or in the dark at 21 °C for 7 d.

Analog Analysis for Quinoxyphen, 4-(2-bromo-4,5-dimethoxy-phenyl)-3,4-dihydro-1H-benzo-quinolin-2-one Action Mechanism. To explore the basis for quinoxyphen activity and determine whether a more potent analog could be identified, a structure-based analysis was conducted using tools available through ChemMine (7) and analogs tested for their ability to inhibit root growth (Fig. S1; analogs listed in Table S1). The analog study led to the observation that 5 of the 6 most active compounds contained an arylbromine group associated with a dimethoxy substitution (Fig. S1; compounds 1, 2, 4, 5, 6). The ortho substituted bromine atom is predicted to withdraw charge from the lone aryl group; specifically, the van der Waals interaction of the relatively large bromine atom overlaps with the protons on the CH_2 group adjacent to the carbonyl. To determine whether other electron-withdrawing groups might phenocopy the aryl bromine-containing quinoxyphen, we assayed an additional set of analogs containing bromo, iodo, nitro, and chloro substitutions (Fig. S1). The substitution of bromine with similar electron-spreading atoms resulted in compounds that also caused significantly shorter and more swollen root and hypocotyl cells. The most potent of these compounds were a 2,3-dichloro (compound 3), 2-chloro-6-fluoro (compound 7), 2-fluoro-5-bromo (compound 13), 6-nitro-1,3-benzodioxol (compound 14) or 2-chloro substitution (compound 15) (Fig. S1*A*). Hence, out of 18 compounds that caused reduced root growth, 15 contained a bromo- or related electron-withdrawing substitution. Overall, far greater concentrations of analogs were needed to assay inhibition of radical elongation than was required for quinoxyphen action (25 μM vs. 1–5 μM); hence, quinoxyphen with its specifically positioned aryl bromine was the most effective of the tested compounds for inhibition of radical elongation.

FTIR Analysis. For Fourier transform infrared (FTIR) analysis, dried WT seedlings (3-d old) grown in 5.0 μM quinoxyphen were pooled and homogenized by ball milling. The powder was dried at 30 °C overnight, mixed with KBr, and pressed into 13-mm pellets. Fifteen FTIR spectra for each line were collected on a Thermo Nicolet Nexus 470 spectrometer (ThermoElectric Corporation) over the range 4,000–400 cm^{-1}. For each spectrum, 32 scans were coadded at a resolution of 8 cm^{-1} for Fourier transform processing and absorbance spectrum calculation by using OMNIC software (Thermo Nicolet). Spectra were corrected for background

by automatic subtraction and saved in JCAMP.DX format for further analysis. Using Win-Das software (Wiley), spectra were baseline-corrected and were normalized and analyzed by using the principal component (PC) analysis covariance matrix method (8). Figures were processed using Sigma Plot (Microsoft).

Callose and Lignin Staining. WT plants were grown for 5 d in the dark on one-half MS agar plates with or without supplementation of 1.0 μM quinoxyphen. Seedlings were directly spread on slides where the staining components were added followed by a coverslip. Callose staining was done with Aniline Blue Fluorochrome (Sigma-Aldrich) at a concentration of 0.1 $mg\,mL^{-1}$ in 0.07 M sodium phosphate buffer, pH 9. Slides were kept in the dark for 1 h before observation under UV light. Phloroglucinol in a 20% hydrocholoric acid solution was used for lignin staining, and slides were observed after 5 min of staining under white light.

Neutral Sugar Analysis of the Quinoxyphen Resistant Mutants. Neutral sugar composition was determined by HPLC from approximately 500 dark-grown hypocotyls from each plant. Cell wall material was prepared from the hypocotyls as described (9) and three replicates of 4 mg of air-dried cell wall material was then prepared for HPLC analysis as described (10).

Glycosyl Linkage Analysis. For glycosyl linkage analysis 1 mg of each sample was prepared in triplicate. The samples were then suspended in 200 uL of dimethyl sulfoxide. The samples were then stirred for 3 d. The samples were permethylated by the treatment with sodium hydroxide and methyl iodide in dry DMSO (11). The samples were subjected to the NaOH base for 15 min, then methyl iodide was added and left for 45 min. The NaOH was then added for 15 min, and finally more methyl iodide was added for 45 min. This addition of more methyl iodide and NaOH base was to insure complete methylation of the polymer. Following sample workup, the permethylated material was hydrolyzed using 2 M trifluoroacetic acid (2 h in sealed tube at 121 °C), reduced with $NaBD_4$, and acetylated using acetic anhydride/trifluoroacetic acid. The resulting partially methylated alditol acetates (PMAAs) were analyzed on an Agilent 7890 A GC interfaced to a 5975 MSD (mass selective detector, electron impact ionization mode); separation was performed on a 30 m Supelco 2330 bonded phase fused silica capillary column (12).

Enzymatic Digestion and Kinetics of Cellulose Saccharification Efficiency. Identical loadings of semipurified cellulose for wild type, $cesa1^{aegeus}$, and $cesa1^{aegeus}/cesa3^{ixr1\text{-}2}$, were analyzed for recalcitrance to saccharification using a commercial cellulase cocktail and compared with the previously measured $cesa3^{ixr1\text{-}2}$ (13). The nature of the improved conversion efficiency was quantified by determining pseudoapparent Michaelis–Menten kinetic parameters recognizing that there are inherent ambiguities with an insoluble substrate like cellulose and a multienzyme cellulase cocktail. Nevertheless, using this method we are able to calculate a K_{cat} value, which represents the most effective measure of substrate performance.

Statistical Analyses. Crystalline cellulose content, glycosidic linkage analysis, neutral sugar composition of WT seedlings germinated with quinoxyphen versus mock treatment and WT versus mutant seedlings, root length of WT seedlings germinated with the analogs versus mock treatment, hypocotyl and root length of WT versus mutants and the RCI values and crystallite width determined by XRD of WT and mutant plants were compared by two-tailed Student's t tests. The mean velocity of labeled CESA complexes were compared between WT and mutants using a univariate analysis of variance, with Bonferroni post hoc tests.

XRD Analysis. Samples were prepared by oven drying biomass at 60 °C for 36 h. Tissue was then homogenized using an Arthur H. Thomas Company Scientific grinder equipped with a 1-mm sieve. Biomass samples were then contained in a custom built sample holder of pressed boric acid. In brief, plant material was placed into a mold containing a sleeve, and hand pressed with a solid metal plug forming a disk shape. The sleeve and plug were removed, and a boric acid (Fischer) base was then formed by pouring the boric acid over the bottom and sides of the sample and applying 40,000 psi of pressure to the 40×40 mm mold using a Carver Autopellet Press. Samples were pressed to create an even horizontal surface. A Bruker-AXS Discover D8 Diffractometer (Bruker-AXS) was used for wide angle X-ray diffraction with Cu Ka radiation generated at 30 mA and 40 kV. The experiments were carried out using Bragg–Brentano geometries (symmetrical reflection). Diffractograms were collected between 2° and 40° with 0.02° resolution and 2-s exposure time interval for each step (run time, 1 h). Sample rotation to redirect the X-ray beam diffraction site was achieved per replicate. *Arabidopsis* material was grown under both greenhouse and growth chamber for analysis. The data analysis was carried out using the calculation for relative crystallinity index (14) of $RCI = I_{002} - I_{am}/I_{002} \times 100$, where I_{002} is the maximum peak height above baseline at approximately 22.5° and I_{am} is the minimum peak height above the baseline at approximately 18°. Diffractograms were collected in DiffracPlus-XRD Commander software (Bruker-AXS) and minimally processed (baseline identification, noise correction, 3D display, and cropping of RCI signature region) using the EVA and TexEval (Bruker-AXS) software.

1. DeBolt S, et al. (2007) Morlin, an inhibitor of cortical microtubule dynamics and cellulose synthase movement. *Proc Natl Acad Sci USA* 104:5854–5859.
2. Desprez T, et al. (2007) Organization of cellulose synthase complexes involved in primary cell wall synthesis in *Arabidopsis thaliana*. *Proc Natl Acad Sci USA* 104:15572–15577.
3. Paredez AR, Somerville CR, Ehrhardt DW (2006) Visualization of cellulose synthase demonstrates functional association with microtubules. *Science* 312:1491–1495.
4. Updegraff DM (1969) Semimicro determination of cellulose inbiological materials. *Anal. Biochem* 32:420–424.
5. Fagard M, et al. (2000) PROCUSTE1 encodes a cellulose synthase required for normal cell elongation specifically in roots and dark-grown hypocotyls of Arabidopsis. *Plant Cell* 12:2409–2424.
6. Desprez T, et al. (2002) Resistance against herbicide isoxaben and cellulose deficiency caused by distinct mutations in same cellulose synthase isoform CESA6. *Plant Physiol* 128:482–490.
7. Girke T, Cheng L-C, Raikhel N (2005) ChemMine. A compound mining database for chemical genomics. *Plant Physiol* 138:573–577.
8. Kemsley EK (1998) *Discriminant Analysis of Spectroscopic Data* (John Wiley and Sons, Chichester, UK).
9. Dick-Pérez M, et al. (2011) Structure and interactions of plant cell-wall polysaccharides by two- and three-dimensional magic-angle-spinning solid-state NMR. *Biochemistry* 50:989–1000.
10. Mendu V, et al. (2011) Subfunctionalization of cellulose synthases in seed coat epidermal cells mediate secondary radial wall synthesis and mucilage attachment. *Plant Physiol* 157:441–453.
11. Ciucanu I, Kerek F (1984) A simple and rapid method for the permethylation of carbohydrates. *Carbohydr Res* 131:209–217.
12. York WS, Darvill AG, McNeil M, Stevenson TT, Albersheim P (1986) Isolation and characterization of plant cell walls and cell wall components. *Methods in Enzymology*, ed Arthur Weissbach HW (Academic, New York), Vol 118, pp 3–40.
13. Harris D, Stork J, DeBolt S (2009) Genetic modification in cellulose-synthase reduces crystallinity and improves biochemical conversion to fermentable sugar. *Glob Change Biol Bioenergy* 1:51–61.
14. Segal L, Creely JJ, Martin AE, Conrad CM (1959) An empirical method for estimating the degree of crystallinity of native cellulose using the X-ray diffractometer. *Text Res J* 29:786–794.

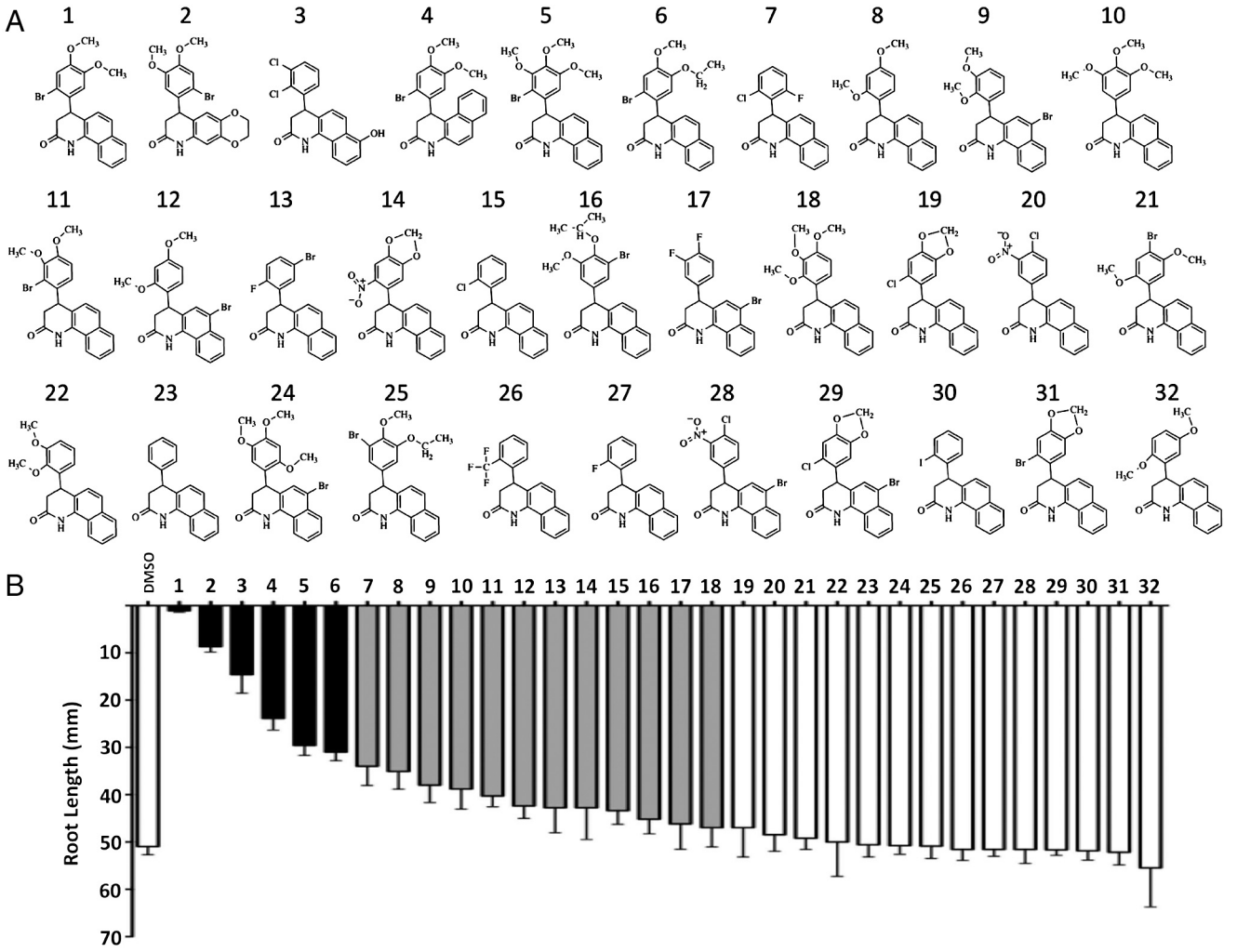

Fig. S1. Analog analysis for quinoxyphen, 4-(2-bromo-4,5-dimethoxy-phenyl)-3,4-dihydro-1H-benzo-quinolin-2-one action mechanism. (*A*) Quinoxyphen (compound 1) and 31 commercially available analogs were identified using webtools available through ChemMine (7). (*B*) Root growth measured as radical elongation was used to assess the potency of each compound at a final concentration of 25 μM. Radical elongation was compared to control with 10 replicates per treatment (error bars indicate one standard deviation from the mean), and colored bars indicate significant reduction in vertical radical length relative to untreated control ($P < 0.05$ Student's t test).

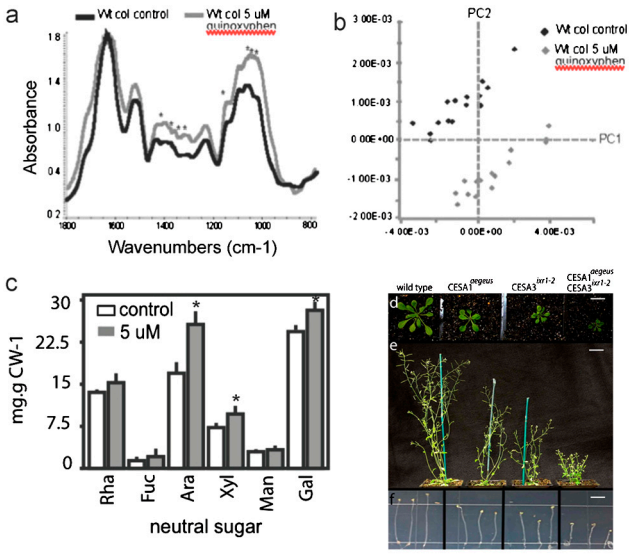

Fig. S2. Effects on cell wall composition following quinoxyphen treatment and mutant phenotype. (*A*) The FTIR spectra of WT seedlings treated and untreated with 5.0 μM quinoxyphen. (*B*) Principal component analysis of the FTIR spectra from the cell walls showed a clear separation of the treated compared with the nontreated seedlings in the first two components (PC). PC 1 and PC 2 explain 93.2% of the variability in the original IR data. Many of the differences between these two samples are present in the fingerprint region of the polysaccharides, although it is difficult to assign to a single cell wall polymer. Absorbance peaks at 1,032, 1,073, and 1,154 cm^{-1} in PC 1 and 991, 1,037, and 1,421 cm^{-1} in PC2 (not shown) are relatively higher in the treated sample compared with the control. In addition, amide-I absorption peak at 1,673 cm^{-1}, stronger in the control sample may reflect higher protein content. (*C*) There was an overall increase in cell wall neutral sugar content of quinoxyphen-treated seedlings compared to the WT control. Specifically, arabinose, xylose, and galactose were significantly higher in the treated seedlings. * Indicates changes were significantly different from WT, $P < 0.05$, Student's *t* test, $n = 3$. (*D–F*) Mutant phenotypes. (*D*) Rosette, (*E*) whole plant, and (*F*) hypocotyl phenotypes of mutants.

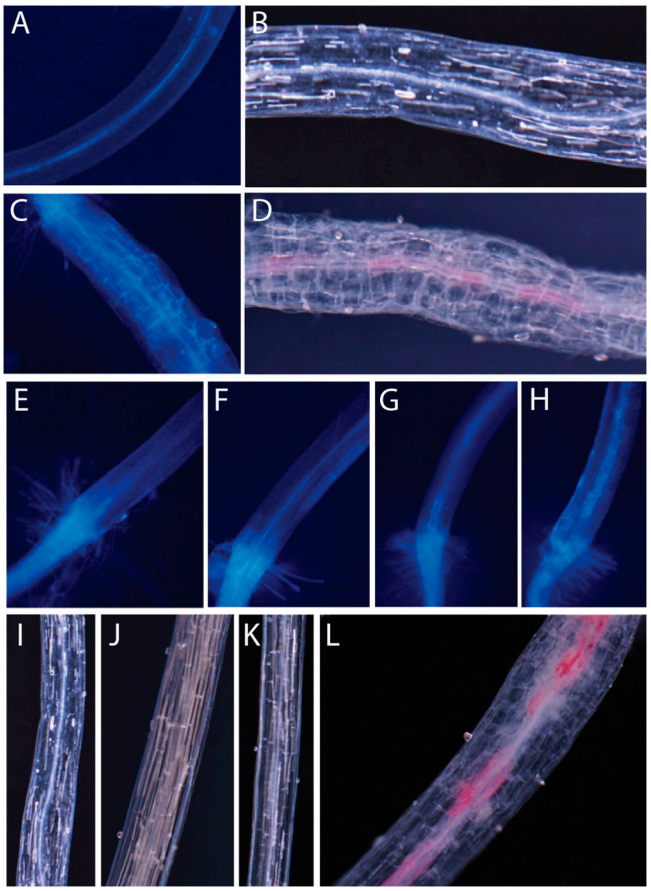

Fig. S3. Hyper-accumulation of callose and ectopic lignin production in mutants and quinoxyphen-treated seedlings. (*A–D*) Dark-grown WT hypocotyls stained with (*A* and *C*) aniline blue indicate an accumulation of callose and with (*B* and *D*) phloroglucinol show an accumulation of lignin when WT seedlings are grown in the presence of 1.0 μM quinoxyphen for 5 d. (*E–H*) Hypocotyls stained with aniline blue. (*E*) WT, (*F*) *cesa1*^{aegeus}, (*G*) *cesa3*$^{ixr1\text{-}2}$, (*H*) *cesa1*^{aegeus}/*cesa3*$^{ixr1\text{-}2}$. (*I–L*) Seven-day-old dark-grown hypocotyls stained with phloroglucinol show no accumulation of lignin in (*I*) WT, (*J*) *cesa1*^{aegeus}, (*K*) *cesa3*$^{ixr1\text{-}2}$, but strong accumulation in (*L*) *cesa1*^{aegeus}/*cesa3*$^{ixr1\text{-}2}$.

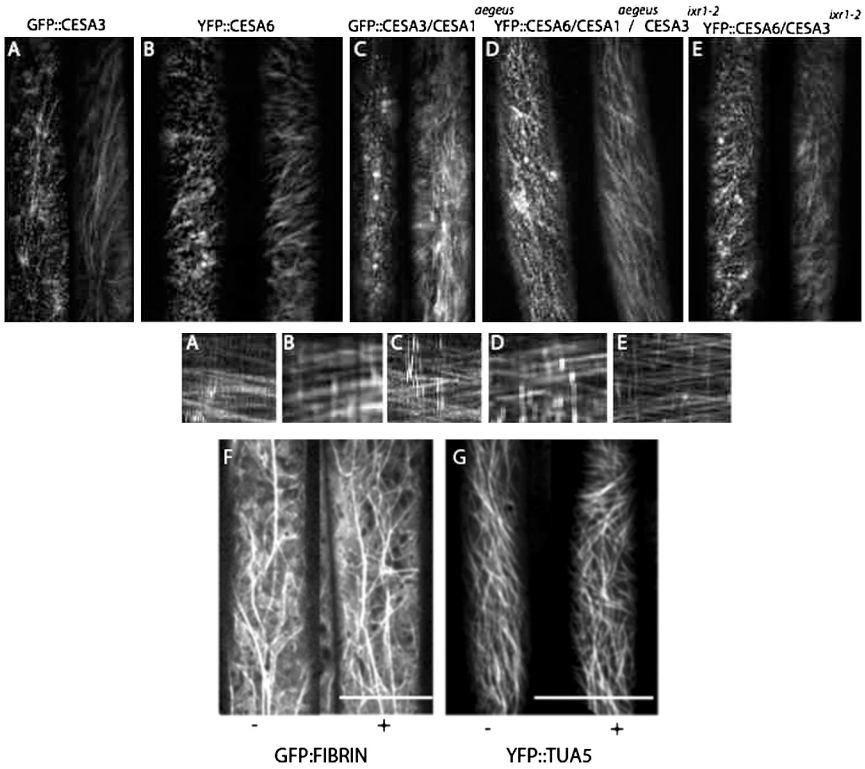

Fig. S4. CESA motility is enhanced in *aegeus* and *ixr1-2* mutants. Transgenic seedlings expressing (*A*) GFP::CESA3, (*B*) YFP::CESA6, (*C*) GFP :: CESA3-*cesa1*^{aegeus}, (*D*) YFP :: CESA6-*cesa1*^{aegeus}/*cesa3*$^{ixr1-2}$ and (*E*) YFP :: CESA6-*cesa3*$^{ixr1-2}$ were grown in the dark for 3 d. Epidermal cells in the upper hypocotyl were imaged with spinning disk confocal microscopy and are presented as both single frame images and time projections (tp) of 72 frames. Time projections are used to create kymographs for PM localized CESA documenting bidirectional velocity (*Inset* for each panel). Quinoxyphen (20 μM) treatment of WT caused no change in morphology or motility of the (*F*) actin cytoskeleton (GFP::FIBRIN) or (*G*) microtubule array (YFP::TUA5).

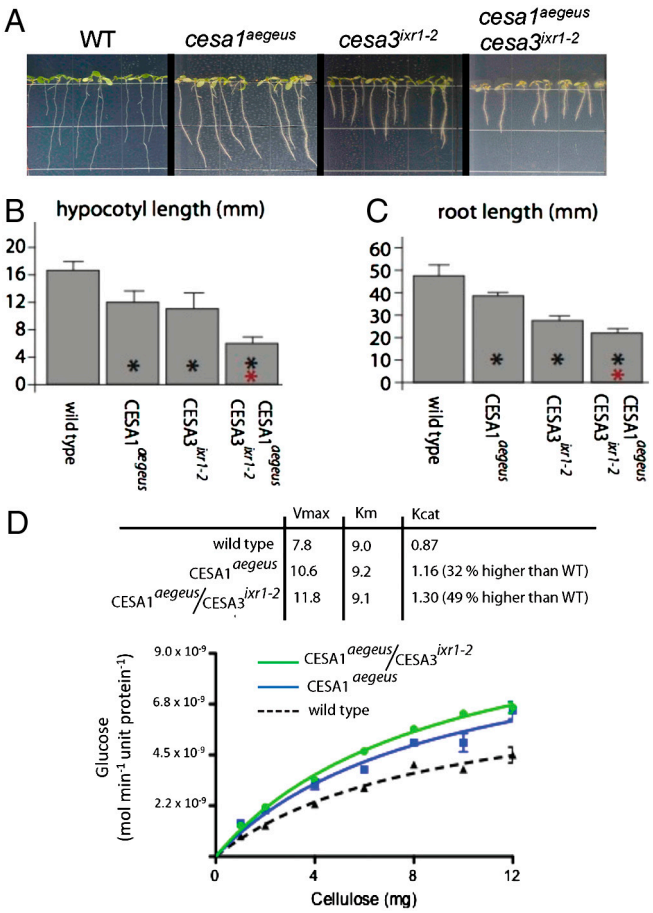

Fig. S5. Phenotypes of *cesa1*^{aegeus} and *cesa3*$^{ixr1\text{-}2}$ mutants. (*A*) The double *cesa1*^{aegeus}/*cesa3*$^{ixr1\text{-}2}$ mutant showed a far more pronounced dwarf phenotype than single mutants in seedling root growth. Measurement of 7-d-old (*B*) hypocotyl and (*C*) root elongation. * Indicates changes were significantly different from WT, $P < 0.05$, Student's *t* test, $n = 10$. (*D*) Enzymatic digestion and kinetics of cellulose saccharification efficiency in mutants containing cellulose structural variation. Pseudoapparent K_m (K'_m) values were determined in the present study for wild-type, *cesa1*^{aegeus} and *cesa1*^{aegeus}/*cesa3*$^{ixr1\text{-}2}$ samples, corresponding to 9.0 ± 1.8 mg, 9.2 ± 2.3 mg and 9.1 ± 0.9 mg cellulose, respectively. Likewise, WT displayed a V'_{max} of $7.82 \pm 0.8 \times 10^{-9}$ moles min^{-1} $unit^{-1}$ $protein^{-1}$ glucose, *cesa1*^{aegeus} displayed a V'_{max} of $10.6 \pm 1.4 \times 10^{-9}$ moles min^{-1} $unit^{-1}$ $protein^{-1}$ glucose, and *cesa1*^{aegeus}/*cesa3*$^{ixr1\text{-}2}$ displayed a V'_{max} of $11.8 \pm 0.6 \times 10^{-9}$ moles min^{-1} $unit^{-1}$ $protein^{-1}$ glucose. These values represents an improvement of 17%, 32%, and 49% for *cesa3*$^{ixr1\text{-}2}$, *cesa1*^{aegeus}, and *cesa1*^{aegeus}/*cesa3*$^{ixr1\text{-}2}$, respectively, in the hydrolytic efficiency of the reaction.

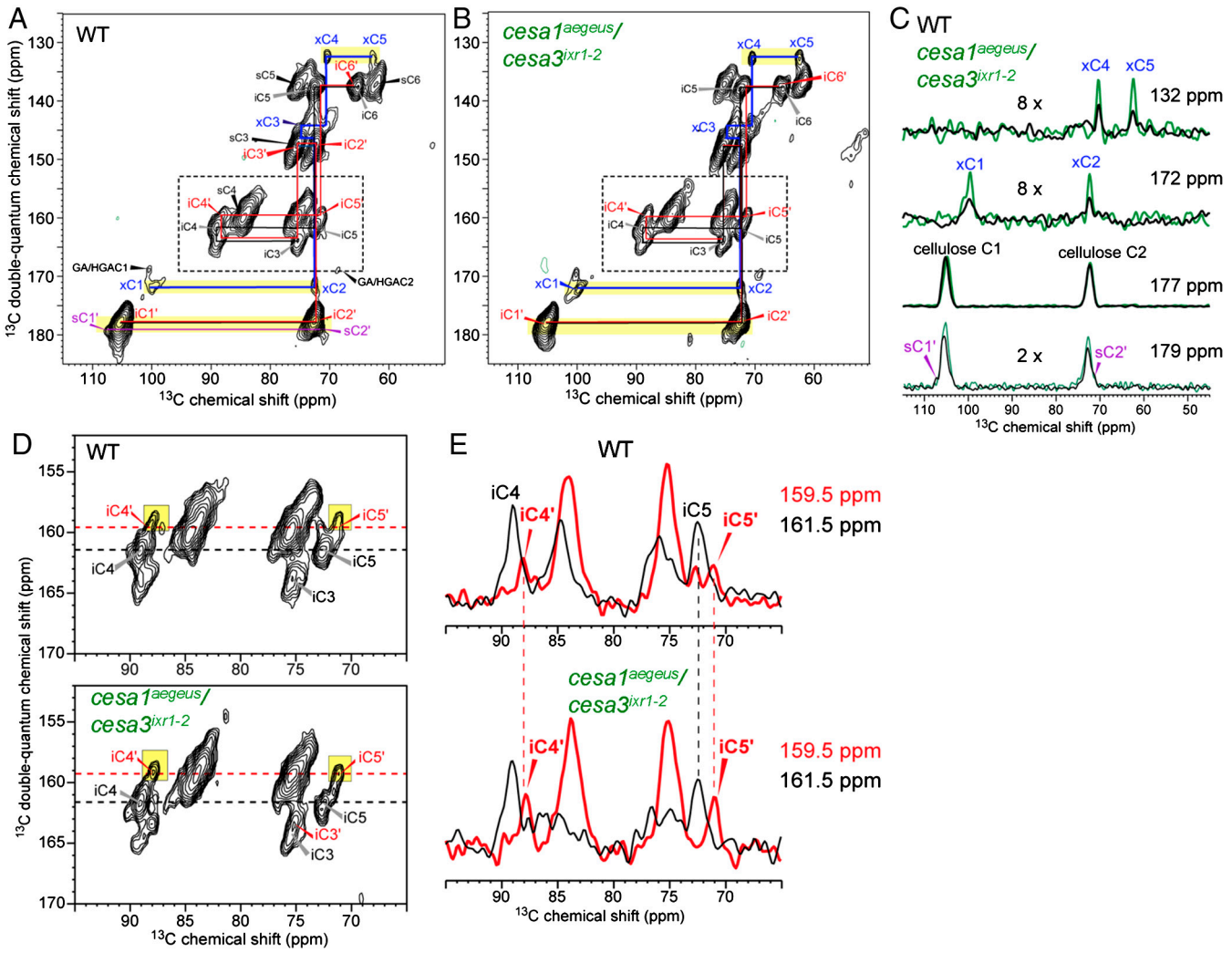

Fig. S6. Two-dimensional ^{13}C double-quantum correlation spectra of WT and *cesa1*^{aegeus}/*cesa3*$^{ixr1\text{-}2}$ cell walls showing changes in the cellulose structure. (*A*) WT cell wall spectrum. Colored assignments denote polysaccharides whose amounts changed in the double mutant. These include xylose (blue), a modified interior cellulose (red with prime) with different C4 and C5 chemical shifts from those of regular crystalline interior cellulose, and a modified surface cellulose (purple with prime) whose C1 and C2 chemical shifts differ from those of regular surface cellulose. (*B*) *cesa1*^{aegeus}/*cesa3*$^{ixr1\text{-}2}$ spectrum. The xylose peaks increased in intensity, the modified surface cellulose signals are absent. (*C*) One-dimensional cross-sections at the specified double-quantum chemical shifts, showing the relative increase of the xylose peak intensities of *cesa1*^{aegeus}/*cesa3*$^{ixr1\text{-}2}$ compared to the WT cell wall and the loss of the modified surface cellulose. (*D*) Expanded C3-C4 and C4-C5 region of the 2D spectra. The C4′ and C5′ peaks of the modified interior cellulose are highlighted in yellow. The intensities of this species relative to the regular interior cellulose are higher in the double mutant than in the WT, which is further shown in the (*E*) 1D cross-sections.

Table S1. Cell wall monosaccharide analysis

Sugar	Wild type	*cesa1*^{aegeus}	*cesa3*$^{ixr1\text{-}2}$	*cesa1*^{aegeus}/*cesa3*$^{ixr1\text{-}2}$
Fucose	0.57 ± 0.15	0.43 ± 0.14	0.53 ± 0.06	0.68 ± 0.11
Rhamnose	16.07 ± 0.75	14.84 ± 0.37*	13.70 ± 0.36*	13.58 ± 0.69*
Arabinose	26.80 ± 0.64	21.99 ± 0.91*	32.46 ± 0.78*	31.00 ± 3.37*
Galactose	23.69 ± 0.40	25.66 ± 0.40*	25.06 ± 0.83*	23.41 ± 1.42
Glucose	2.98 ± 0.24	4.35 ± 0.34*	3.04 ± 0.05	3.86 ± 0.05*
Mannose	6.08 ± 0.63	6.87 ± 0.75	7.28 ± 1.00	8.15 ± 1.56
Xylose	10.43 ± 0.91	7.96 ± 0.12*	8.66 ± 0.51*	8.59 ± 0.59*
GalA	12.85 ± 0.76	9.56 ± 0.39*	8.91 ± 0.59*	10.30 ± 0.98*
GlucA	0.53 ± 0.06	0.46 ± 0.05	0.36 ± 0.06*	0.42 ± 0.07*

The results are expressed in mol %. * Indicates changes were significantly different from WT, $P < 0.05$ Student's *t* test, $n = 3$.

Table S2. Glycosyl linkage analysis

Linkage	WT	*cesa1*^{aegeus}/*cesa3*$^{ixr1\text{-}2}$
t-Fuc	0.67 ± 0.06	0.60 ± 0.00
t-Rha	0.70 ± 0.17	0.63 ± 0.06
2-Rha	1.57 ± 0.15	1.23 ± 0.30
2,4-Rha + 2-Man + 3-Man	1.63 ± 0.06	2.20 ± 0.26*
t-Ara	0.17 ± 0.06	0.20 ± 0.00
t-Araf	2.77 ± 0.85	4.07 ±0.81
2-Araf	2.17 ± 0.64	1.97 ± 0.15
3-Araf	0.83 ± 0.25	0.80 ± 0.10
2,3,4-Ara	0.30 ± 0.14	1.05 ± 1.06
4-Arap or 5-Araf	1.87 ± 0.49	2.53 ± 0.15*
2,4-Arap or 2,5-Araf	1.40 ± 0.53	1.53 ± 0.15
3,4-Arap or 3,5-Araf	0.60 ± 0.20	0.97 ± 0.21*
t-Xyl	2.93 ± 0.57	2.70 ± 0.35
4-Xyl	2.93 ± 0.21	2.27 ± 0.28*
2,4-Xyl	0.83 ± 0.06	1.00 ± 0.17
2,3,4-Xyl	0.10 ± 0.06	0.20 ± 0.14
t-Galf	0.20 ± 0.10	0.30 ± 0.00
t-Gal	3.33 ± 0.57	3.70 ± 0.35
2-Gal	1.53 ± 0.15	1.40 ± 0.30
3-Gal	8.13 ± 1.80	11.87 ± 1.46*
4-Gal	0.83 ± 0.25	1.07 ± 0.21
6-Gal	0.47 ± 0.06	0.63 ± 0.06*
2,3-Gal	0.23 ±0.06	0.33 ± 0.06
3,6-Gal	1.27 ± 0.06	2.30 ± 0.20*
4,6-Gal	0.10 ±0.00	0.17 ± 0.06
3,4,6-Gal	0.20 ± 0.10	0.27 ± 0.12
t-Glc	0.53 ± 0.06	0.60 ± 0.17
2-Glc	0.67 ± 0.35	0.77 ± 0.31
4-Glc	48.97 ± 4.76	41.37 ± 2.17*
2,4-Glc	0.57 ± 0.21	0.43 ± 0.06
3,4-Glc	0.47 ± 0.15	0.40 ± 0.00
4,6-Glc	4.43 ± 0.12	3.63 ± 0.50*
3,4,6-Glc	0.13 ± 0.06	0.10 ± 0.00
2,4,6-Glc	0.13 ± 0.06	0.20 ± 0.17
2,3,6-Glc	N.D.	0.10 ± 0.00
t-Man	1.73 ± 0.38	2.40 ± 0.26*
4-Man	2.73 ± 0.21	2.17 ± 0.25*
4,6-Man	1.63 ± 0.40	1.87 ± 0.06
3,6-Man	0.37 ± 0.12	0.40 ± 0.20

The results are expressed in relative %. * Indicates changes were significantly different from WT, $P < 0.05$ Student's t test, $n = 3$.

Table S3. Relative intensities of interior and surface cellulose C4 signals of different cell walls from quantitative ^{13}C NMR spectra

Genotype	I(iC4) 88.5–91.5 ppm	I(sC4) 84–86 ppm	I(iC4)/I(sC4)	Normalized I(iC4)/I(sC4)
Wild type	37.7E6	58.1E6	0.65	1.00
cesa1^{aegeus}	22.4E6	32.7E6	0.69	1.06
cesa3$^{ixr1\text{-}2}$	25.1E6	39.3E6	0.64	0.98
cesa1^{aegeus}/*cesa3*$^{ixr1\text{-}2}$	19.1E6	32.0E6	0.60	0.92

cesa1^{aegeus}/*cesa3*$^{ixr1\text{-}2}$ cell wall exhibits a clear reduction in crystallinity.